Journal of the Korean Society for Nondestructive Testing
Vol. 26, No. 6 (2006. 12)

Inspection of Ceramic Coatings Using Nanoindentation and Frequency Domain Photoacoustic Microscopy

T.L. Steen*, S.N. Basu**, V.K Sarin** and T.W. Murray*,†

Abstract The elastic properties and thickness of mullite environmental barrier coatings grown through chemical vapor deposition (CVD) on silicon carbide substrates were measured using frequency domain photoacoustic microscopy. In this technique, extremely narrow bandwidth surface acoustic waves are generated with an amplitude modulated laser source. A photorefractive crystal based interferometer is used to detect the resulting surface displacement. The complex displacement field is mapped as a function of source-to-receiver distance in order to extract the wavelength of the surface acoustic wave at a given excitation frequency, and the phase velocity is determined. The coatings tested exhibited spatial variations in thickness and mechanical properties. The measured surface wave dispersion curves were used to extract an effective value for the elastic modulus and the coating thickness. Nanoindentation was used to validate the measurements of the effective elastic modulus. The average elastic modulus measured through the coating thickness using nanoindentation is compared to the effective modulus found using the photoacoustic system. Optical microscopy is used to validate the thickness measurements. The results indicate that the photoacoustic microscopy technique can be used to estimate the effective elastic properties in coatings exhibiting spatial inhomogeneities, potentially providing valuable feedback for the optimization of the CVD growth process.

Keywords: Laser Ultrasonics, Nanoindentation, Coating Inspection, Optical Metrology

1. Introduction

Silicon based ceramics, such as SiC and Si_3N_4, are promising materials for high temperature applications due to their high temperature stability, strength, and oxidation resistance, as well as their low coefficient of thermal expansion (CTE). Environmental barrier coatings can be used to limit the high temperature corrosion and recession of these materials. Mullite ($3Al_2O_3 \cdot 2SiO_2$) is a suitable coating for silicon-based ceramics because of its high temperature strength, corrosion resistance, and excellent CTE match with SiC. Chemical vapor deposition (CVD) can be used to grow mullite coatings on SiC substrates with complex geometries (Hou et al., 2001). In addition, it has been shown that by altering the growth conditions, mullite coatings can be grown over a wide range of compositions. This opens up the possibility of functionally grading coatings such that they offer maximum protection against corrosion and recession at the coating surface, while having an optimum thermal expansion match with the substrate at the interface.

In order to optimize the growth parameters in the CVD reactor, it is necessary to provide feedback of coating quality through analysis of

Received: October 16, 2006, Accepted: Novemver 25, 2006. * Department of Aerospace and Mechanical Engineering ** Department of Manufacturing Engineering, 110 Cummington Street, Boston University, Boston MA 02215 USA, † Corresponding author: twmurray@bu.edu

the mechanical and dimensional properties. A wide variety of experimental tools have been developed for coating characterization including surface Brillouin scattering (Berezina et al., 2004; Briggs, 1995), conventional acoustic microscopy (Briggs, 1995, 1992; Guo and Achenbach, 2000), indentation techniques, and laser based ultrasonic techniques. Laser based ultrasonic techniques, which use optical sources for the generation and detection of ultrasound, have seen widespread use for the inspection of coating materials. In general, laser based ultrasonic techniques that have been developed for coating inspection fall into two general categories: bulk wave based measurement systems using ultrafast laser sources (Maris, 1997; Richardson et al., 1999) and surface acoustic wave (SAW) measurement systems. In bulk wave measurement systems, a picosecond or femtosecond laser source is used to launch GHz range longitudinal waves into the coating, which reflect from the interface with the substrate and are detected at the coating surface. This technique has seen extensive use for the inspection of thin films used in the semiconductor industry. Attenuation of the high frequency bulk waves places some limitations on the use of this technique for the inspection of thick (micron scale) coatings. In the second technique, SAWs are generated in the coating using a pulsed picosecond or nanosecond laser source (Duggal et al., 1992; Hurley et al., 2001; Neubrand and Hess, 1992; Rogers et al., 2000; Murray et al., 2005). The phase velocity of the SAWs is measured as a function of frequency to obtain the dispersion characteristics. The measured dispersion behavior is then compared to a theoretical model in order to determine the properties of the coating.

While laser based ultrasonic systems allow for the non-contact generation and detection of acoustic waves over a wide range of frequencies, making them particularly attractive for in-situ measurement applications, the sensitivity of these systems may be insufficient for some applications. On the generation side, the maximum ultrasonic displacement is limited by the amount of light that can be absorbed by the specimen surface without causing irreversible damage to the coating. On the detection side, the displacement sensitivity is limited by the amount of light that can be collected from the specimen surface and by the overall bandwidth of the detection system. The latter limitation is particularly important because coating inspection utilizes high frequency ultrasound. Using a pulsed laser source, the ultrasonic energy is spread over a wide frequency band, and the detection system must be matched to that of the ultrasound. This makes the detection system susceptible to broadband thermal and quantum noise.

We have recently developed a new laser based ultrasonic approach, referred to as frequency domain photoacoustic microscopy, for high frequency acoustic wave generation and detection, which allows for the measurement of very small surface displacements, generated with only moderate surface heating (Balogun and Murray, 2006; Murray and Balogun, 2004). Instead of using a pulsed laser source for the excitation of acoustic waves, the system uses an amplitude modulated continuous wave laser. The use of a sinusoidally modulated laser source allows for the generation of acoustic waves with an extremely narrow-bandwidth. For coating inspection, the amplitude modulated laser source has been combined with a photorefractive crystal based optical interferometry system, allowing for the detection of surface acoustic waves at frequencies up to 200 MHz on optically rough surfaces. The output of the interferometer is measured using a radio frequency (RF) lock-in amplifier. The displacement sensitivity of the system is controlled by the integration time of the lock-in, allowing for a trade off between signal-to-noise ratio and measurement time. The generation and detection laser sources are focused to the surface through a single

microscope objective allowing for highly localized (over a source-to-receiver distance of approximately 600 μm) measurements of coating properties. The SAW phase velocity is measured by holding the excitation source at a fixed temporal frequency as it is scanned across the specimen surface. At each temporal frequency of interest, the spatial frequencies of the SAW modes present in the system are found, from which the phase velocity can be determined. Velocity measurements are performed at multiple frequencies until the dispersion relation is constructed over the desired bandwidth. A theoretical dispersion curve is then fit to the experimental dispersion curve to extract the chosen mechanical and dimensional properties of the coating.

In this paper, frequency domain photoacoustic microscopy is used to measure the thickness and elastic modulus of *as-grown* CVD mullite coatings on SiC substrates. The coatings selected for this study were deposited on unpolished substrates and have optically rough surfaces. In addition, the coatings show some variation in thickness across the surface and have a gradation in elastic properties through the coating thickness. In general, it would be desirable to use the photoacoustic technique to measure both the local change in elastic properties through the thickness of the coating and the more gradual changes in thickness across the surface. While the theory for SAWs in multilayer structures is well-established (Farnell and Adler, 1972) and can be applied to coatings with property gradations through the coating thickness, the spatial inhomogeneities that can occur in coatings grown during the optimization of a growth process, as well a limited knowledge of any of the coating mechanical properties, restricts the amount of information that can be obtained from a SAW dispersion measurement. However, the dispersion behavior of the SAWs can be used to estimate an effective elastic modulus through the coating and to estimate the coating thickness. These are both valuable parameters that may provide sufficient information to make determinations regarding the coating quality. In this work, we treat the material system as a single homogeneous, isotropic coating on a semi-infinite substrate. In this case, the dispersion relation can be written in the general form:

$$V(f) = f\lambda = V\left(E_c, E_s, \rho_c, \rho_s, \nu_c, \nu_s, \frac{t}{\lambda}\right) \qquad (1)$$

where $V(f)$ is the SAW velocity as a function of frequency. The SAW velocity is dependant on the Young's moduli (E_c, E_s), densities (ρ_c, ρ_s), and Poisson's ratios (ν_c, ν_s) of the coating and substrate, as well as the ratio of the coating thickness to wavelength (t/λ). The actual dispersion relation is found by solving the equations of elasticity subject to the appropriate boundary conditions at the coating surface and interface with the substrate as described in detail in the literature (Cheng et al., 2001).

In order to validate the photoacoustic results, two additional experimental techniques are employed: nanoindentation and optical microscopy. Nanoindentation is a well established technique for determining coating properties (Doerner and Nix, 1986; Ziebert et al., 2006) and has been previously used in conjunction with laser based ultrasonic techniques for coating inspection (Vaz et al., 2002; Zhang et al., 2006). Nanoindentation measurements are made on polished cross-sections of the coating to determine modulus variations through the coating thickness. These measurements are performed in the same coating areas as the photoacoustic measurements, and the effective elastic modulus measured using the photoacoustic technique is compared to the mean elastic modulus in the coating determined by nanoindentation. While nanoindentation is an excellent technique to measure the spatially resolved mechanical properties of coatings, it requires a significant amount of specimen preparation (in the case of cross sectional measurements) and is not well suited for in-situ

process control. In principle, it is also possible to measure elastic property variations in coatings through indenting the top of the coating, rather than taking measurements on the cross section (Bellan and Dhers, 2004; Ohmura and Matsuoka, 2003). However, in the present case this approach is not applicable due to high surface roughness. In order to measure the thickness of the coating, polished coating cross-sections are examined by optical microscopy. Again, measurements are taken at the same regions of the coating as the photoacoustic measurements, and the results are compared.

2. Experimental Methods

2.1 Frequency Domain Photoacoustic Microscopy

A schematic of the frequency domain photoacoustic microscopy system is given in Fig. 1. The system consists of two optical paths that lead to the specimen surface: the generation beam path and the detection beam path. The generation beam path delivers an amplitude modulated laser source to the specimen surface. The generation laser is an electro-absorptive modulated diode laser (EML) operating at 1550 nm with an output power of 1 mW. A signal generator is used to sinusoidally modulate the output intensity of the EML, which has a modulation bandwidth of 2.0 GHz. The output from the EML is coupled through an optical fiber to an erbium doped fiber laser amplifier (EDFA). The EDFA is capable of amplifying the laser intensity up to 5 W. Out of the amplifier, a beam sampler is placed in the beam path to gather a small portion of the beam for use as a reference signal in the lock-in amplifier. The beam is then reflected off a mirror mounted on a gimbal mount and directed through two relay lenses. The beam is subsequently focused onto the specimen surface through a long working distance objective (LWDO) with a numerical aperture (NA) of 0.40. The average generation power at the specimen surface was measured to be approximately 800 mW. The gimbal scanning mirror, the two relay lenses, and the back aperture of the objective are positioned as a 4f system. This configuration allows for the translation of the generation beam focal position on the specimen surface through the controlled rotation of the gimbal scanning mirror.

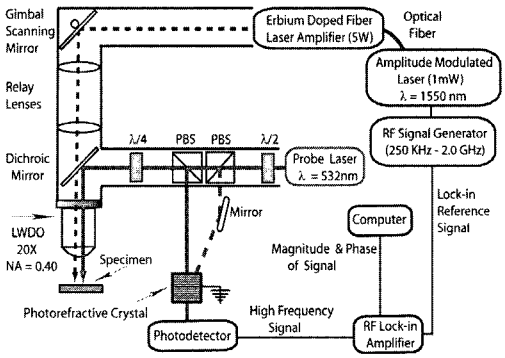

Fig. 1 Schematic of the photoacoustic microscopy system, with the following components indicated: PBS (polarizing beam splitter), LWDO (long working distance objective), λ/2 (half wave plate), λ/4 (quarter wave plate).

The normal displacement of the specimen is detected using a photorefractive crystal (PRC) based interferometer. The detection laser is a Nd:YAG operating at 532 nm with an optical power of 220 mW. The detection beam enters the photoacoustic microscopy system through a half-waveplate and a polarizing beamsplitter (PBS), the combination of which acts as a variable attenuator. At the PBS, the beam is split into a signal and reference beam. The signal beam is directed through the LWDO and focused on the specimen surface. Upon reflection from the specimen, the signal beam is recombined with the reference beam in the PRC for adaptive holographic detection of the surface displacements. After the crystal, the detection beam is directed into a photodetector, from which the high frequency signal is sent to a

lock-in amplifier operating at a detection bandwidth of 1.6 Hz. At the lock-in amplifier, the magnitude and phase of the signal are measured at the modulation frequency of the generation beam.

An adaptive PRC based detection scheme has been selected for this work due to the high surface roughness exhibited by the coating specimens. PRC based interferometers have seen widespread use in the optical detection of ultrasound and are well suited for the detection of vibrations from rough surfaces (Blouin and Monchalin, 1994; Delaye et al., 1997; Ing and Monchalin, 1991). A brief description of the operation of the interferometer follows. The signal beam reflected from the specimen surface acquires a phase due to interaction with the ultrasound. The signal beam is then mixed with a reference (or pump) beam inside the PRC. The mixing of the signal and reference beam creates an interference pattern in the crystal. Free carriers are excited in the bright regions of the intensity pattern, which then diffuse or drift to the dark regions. This drift of free carriers leads to the formation of a space-charge field within the crystal and modulates the index of refraction through the electro-optic effect. When the reference beam interacts with the index of refraction grating in the crystal, a portion is diffracted into the signal beam path providing a wavefront matched reference beam. The reference beam that has been diffracted into the signal beam path has the same phase front as the signal beam, independent of speckle structure. After the PRC, the signal and reference beams interfere, and the phase modulation in the signal beam results in an intensity change at the detector. A bismuth silicon oxide (BSO) photorefractive crystal is used with dimensions of 0.5 x 0.5 x 0.7 cm. A 4 kV/cm DC electric field is applied to the crystal, bringing the phase between the diffracted reference and the signal beam to near quadrature, which is where the interferometer is most sensitive to phase modulation.

To make SAW phase velocity measurements, the generation laser is held at a fixed modulation frequency and scanned over the specimen surface in discrete steps. The complex amplitude of the normal displacement of the specimen surface at each source-to-receiver position is measured. As the source-to-receiver distance is increased, the phase of the SAW is delayed, or in terms of the complex amplitude, the real and imaginary components of displacement show periodic behavior. These components exhibit one full cycle of oscillation when the source-to-receiver distance is changed by one wavelength. In order to measure the SAW phase velocity (V) using this technique, the wavelength (λ) of the SAW is measured at a given frequency (f) and the velocity is found through:

$$V = f\lambda \tag{2}$$

A Fourier transform can be used to convert the complex amplitude $u_z(r)$ measured as a function of space to a complex amplitude $F(k_s)$ as a function of spatial frequency (k_s) as follows:

$$F(k_s) = \int_{-\infty}^{\infty} u_z(r) e^{-ik_s r} dr \tag{3}$$

This approach is similar to that followed by Alleyne and Cawley (Alleyne and Cawley, 1991). A plot of the magnitude of the signal as a function of spatial frequency reveals peaks corresponding to propagating acoustic modes. The wavelength of each acoustic mode is then given by:

$$\lambda = \frac{2\pi}{k_s} \tag{4}$$

To demonstrate this measurement technique, the complex displacement of SAWs excited in an aluminum alloy-6061 specimen at a frequency of 100 MHz is plotted in Fig. 2(a). These measurements were made on the specimen surface at 95 spatial positions separated by 4.7 μm starting at a source-to-receiver distance of 40 μm.

It can be observed in Fig. 2(a) that the real and imaginary components of the normal displacement oscillate as the source-to-receiver distance is increased. A Fourier transform was applied to the complex displacement data in Fig. 2(a) and the magnitude is presented in Fig. 2(b). A strong peak at a spatial frequency of 34.18 mm^{-1} is observed, corresponding to an acoustic wavelength of 29.25 μm. In this case, with an excitation temporal frequency of 100 MHz, the velocity was found to be 2925 m/s.

This procedure for data acquisition and analysis is used to calculate the velocity of SAW modes generated in the mullite coating/SiC substrate specimens. The dispersion relation in these specimens is found by taking SAW velocity measurements at multiple temporal frequencies

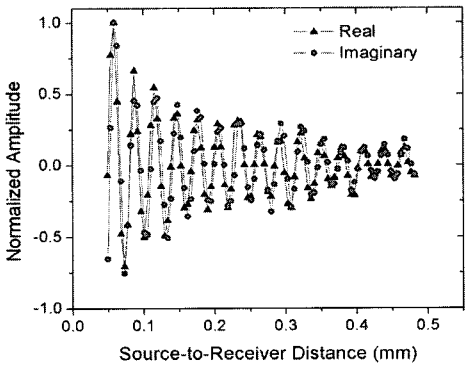

(a)

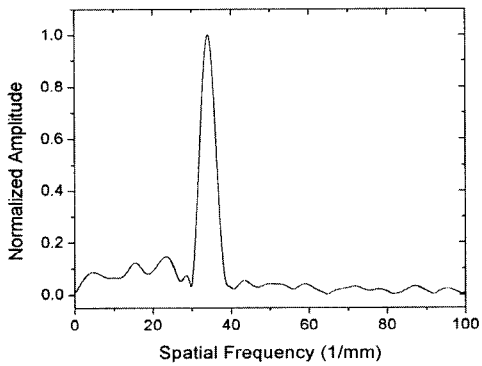

(b)

Fig. 2 (a) Complex amplitude of the ultrasonic displacement as a function of source-to-receiver distance. (b) Magnitude of the Fourier transform of the measured data.

over the desired bandwidth. To estimate the coating properties of interest, the experimental dispersion curves are fit to theoretical dispersion curves produced using a model of a single layered coating on a semi-infinite substrate. The simplex algorithm is used to minimize the error between calculated and measured dispersion curves (Flannery et al., 1989).

2.2 Nanoindentation

Nanoindentation measurements are performed on polished cross-sections of mullite coatings using a Hysitron Triboindenter® with a diamond Berkovich tip. Fig. 3 is an example of an array of indents throughout the thickness of a coating cross-section. Fig. 4 is a sample load-displacement curve from an indent performed in a SiC specimen. In this curve, the load of the indenter tip on the specimen is increased at a rate of 1000 μN/s to a maximum load (P_{max}) of 5000 μN where the specimen reaches its maximum displacement (h_{max}) of 91nm. The load displacement curves are analyzed using the Oliver – Pharr method (Oliver and Pharr, 1992) to extract the reduced modulus of the specimen. The first step in the analysis is to determine the initial unloading contact stiffness S by calculating the slope of the initial unloading curve. The initial contact stiffness is used in eqn. (5) to calculate the contact depth h_c.

$$h_c = h_{\max} - 0.75\frac{P_{\max}}{S} \tag{5}$$

The reduced modulus E_r of the material is then calculated using eqn. (6).

$$E_r = \frac{\sqrt{\pi}}{2\sqrt{A(h_c)}}S \tag{6}$$

Where $A(h_c)$ is the area function of the indenter tip that provides a numerical relationship between the contact depth and the tip area. The elastic modulus of the specimen $E_{specimen}$ can be calculated using eqn. (7).

$$\frac{1}{E_r} = \left(\frac{1-\nu^2}{E}\right)_{Specimen} + \left(\frac{1-\nu^2}{E}\right)_{Indenter} \quad (7)$$

In eqn. (7), the indenter has the properties of diamond ($\nu_{Indenter}$ = 0.07, $E_{Indenter}$ = 1140 GPa) and the Poisson's ratio of the specimen must be assumed. In this work, the Poisson's ratio of mullite is assumed to be 0.28 (Ledbetter et al., 1998).

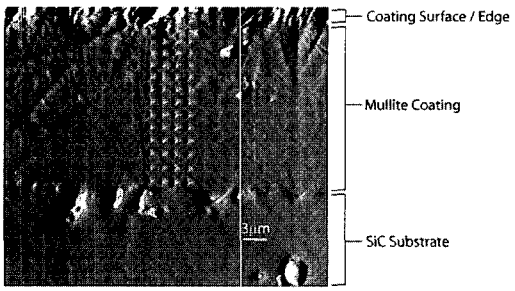

Fig. 3 Sample array of indents performed throughout the thickness of a mullite coating.

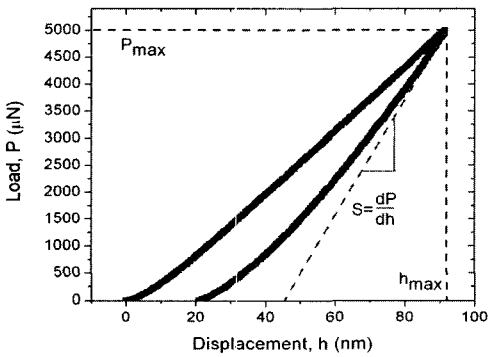

Fig. 4 Example of a load-displacement curve extracted from an indent on a SiC specimen.

3. Results and Discussion

Prior to coating inspection, measurements were performed on a silicon wafer with a known SAW velocity to calibrate the source-to-receiver step size in the photoacoustic microscopy system. After the system calibration, SAW velocity measurements were performed on an aluminum alloy-6061 specimen to investigate the accuracy of the phase velocity measurements. SAWs propagating on a homogenous, semi-infinite half space are not expected to exhibit dispersion. The SAW phase velocity was measured over a frequency range of 100 MHz to 200 MHz in 25 MHz steps with ten measurements at each frequency. The mean SAW velocity over this range was 2927.4 m/s. The velocity measurements at each frequency have extremely low standard deviations, typically on the order of 0.5m/s. However, there was some discrepancy in the mean velocities measured at each frequency, with the standard deviation of the five recorded mean values falling at 2.4 m/s. The reason for the larger variation in the mean values is unclear and could be either a systematic error in the measurement or a specimen effect such as finite surface roughness.

Photoacoustic and nanoindentation measurements were performed on CVD mullite coatings deposited on 3 × 4 × 20 mm^3 SiC substrates. A 1 mm thick cross-section was cut from the end of the specimen with a diamond saw blade, and was manually polished using a 0.5 μm diamond abrasive film disc. The cross-section was used to observe the thickness and uniformity of the coating under an optical microscope with a magnification of 500 x. A sample image from the optical microscope can be seen in Fig. 5. The side of the coating with the most uniform thickness was selected for analysis. Nanoindentation and photoacoustic measurements were made in three regions across the cross-section as indicated by the schematic in Fig. 6. Observations using the optical microscope indicate that the coating thickness on the selected face varied from 10 μm in Region 1 to 15 μm in Region 3.

To extract the depth profile of the elastic modulus in the mullite coatings, an array of indents was performed throughout the entire thickness of the coating cross-section. Two nanoindentation arrays were made in each of the measurement regions indicated in Fig. 6. Indents

were performed with a maximum load of 5000 μN. All arrays were composed of four indents at each depth with a separation of 1.7 μm between the rows and columns. The mean value of the elastic modulus as a function of distance from the coating/substrate interface was then calculated. Fig. 7(a) displays a sample elastic modulus profile from an array of indents in Region 3 with the error bars representing the standard deviation of the four indents at each depth. It can be seen in Fig. 7(a) that the elastic modulus of the coating at this location increases from 150 GPa at the coating/substrate interface to 190 GPa at the coating surface.

Photoacoustic experiments were performed on the bulk specimen, at positions adjacent to where the nanoindentation measurements were performed in the cross-section. The dispersion curves measured using the photoacoustic microscopy system were fit to the theoretical model to extract the effective elastic modulus and thickness of the coating over the inspection area. The mechanical properties used in the model were the Poisson's ratio (0.28) and density (3156 kg/m^3) of the mullite coating, as well as the Poisson's ratio (0.14) and density (3100 kg/m^3) of the substrate. The SAW velocity of the SiC substrate was determined experimentally to be 6925 m/s. In the mullite specimen, SAW velocity measurements were performed in steps of 25 MHz over a frequency range of 100 MHz to 200 MHz. Two measurements were taken in each of the three regions illustrated in Fig. 6. A representative

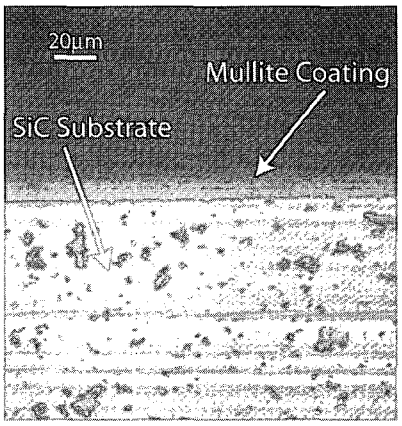

Fig. 5 Image of a polished coating cross section from an optical microscope with a magnification of 500x.

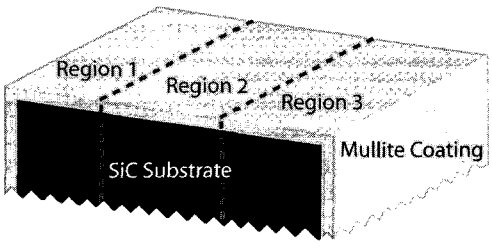

Fig. 6 Location of the measurements on selected side of the specimen.

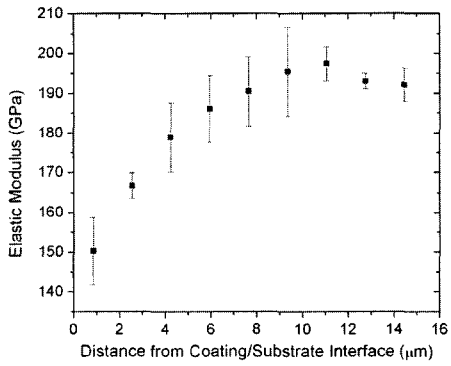

(a)

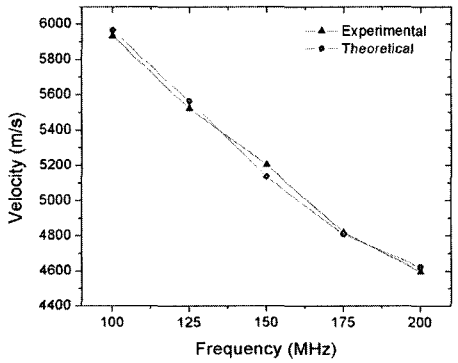

(b)

Fig. 7. (a) Depth distribution of the elastic modulus in the mullite coating from nanoindentation measurements in Region 3. (b) Experimental and theoretical dispersion curve from Region 2.

dispersion curve from Region 2 is presented in Fig. 7(b). The effective properties of the mullite coating resulting from the fitting of this dispersion curve are E = 177.5 GPa and thickness = 13.4 μm.

Fig. 8(a) is a comparison between the coating elastic modulus measured using the photoacoustic microscopy system and nanoindentation in each region of the specimen. The elastic modulus values displayed for the photoacoustic technique represent the mean elastic modulus from the two measurement locations in each region. The elastic modulus displayed for nanoindentation represents the mean value of all indents made throughout the thickness of the coating in each region. The error bars for both techniques represent the standard deviation of the measurements in each region. Fig. 8(a) shows a general agreement between the two techniques, both showing a trend of increasing elastic modulus from Region 1 to Region 3. The maximum discrepancy occurs in Region 2 where the mean elastic modulus value from nanoindentation is 9% lower than the mean effective modulus found using the photoacoustic technique. Nevertheless, the agreement is very reasonable considering the complex structure of the coating, and the fact that the coating is modeled as a homogeneous single layer. Fig. 8(b) is a comparison of the coating thickness measured using the photoacoustic microscopy system and observations with the optical microscope. The thickness value displayed for the photoacoustic technique is the mean thickness extracted from the two measurement locations in each region. The error bars for the photoacoustic values represent the standard deviation of the measurements in each region. The thickness value displayed for optical microscopy is the coating thickness at the center of each region. Fig. 8(b) demonstrates agreement between the two techniques, showing a trend of increasing coating thickness from Region 1 to Region 3. The maximum discrepancy occurs in Region 1 where the thickness value obtained using the optical microscope is 14% lower than the photoacoustic technique.

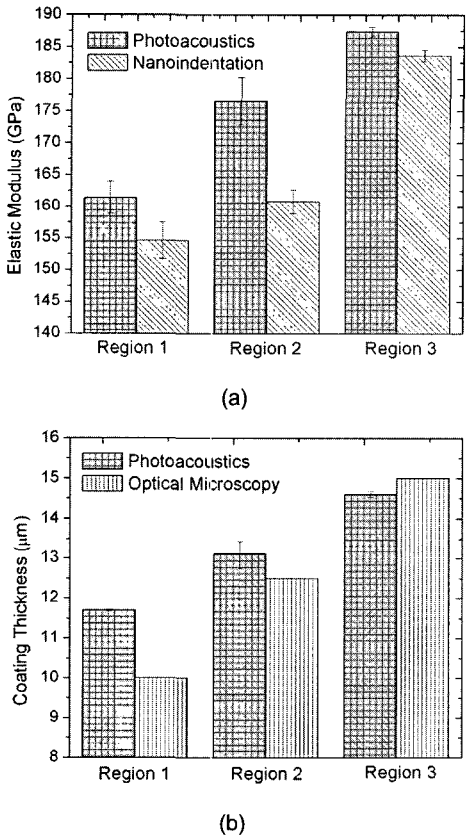

Fig. 8 (a) Comparison of the elastic modulus of the coating found using nanoindentation and photoacoustics. (b) Comparison the coating thickness found using photoacoustics and the optical microscope.

In a separate area of the specimen, an additional point-by-point inspection of the elastic modulus and thickness of the coating was performed. Photoacoustics and nanoindentation measurements were made at nine positions across the specimen in uniform steps of 250μm. A schematic of this experiment is illustrated in Fig. 9. Measurements using the photoacoustic microscopy system were performed on the bulk specimen before a cross-section was removed. Upon completion of the photoacoustic measurements, the specimen was cut directly where the photoacoustic measurements had been performed. A polished cross-section of the

specimen was then prepared for optical observation and nanoindentation measurements.

Photoacoustic experiments were performed on the bulk specimen at each position as illustrated in Fig. 9. SAW dispersion curves were analyzed to extract the effective elastic modulus and thickness of the coating over the inspection area. SAW velocity measurements were performed in steps of 25 MHz over a frequency range of 100 MHz to 200 MHz. A representative dispersion curve from position 9 is presented in Fig. 10(b). The effective properties of the mullite coating resulting from fitting this dispersion curve are E = 175.9 GPa and thickness = 12.5 μm.

Nanoindentation measurements were performed on the polished cross-section at each position as illustrated in Fig. 9. Indents were executed with a maximum load of 5000 μN. All arrays were composed of four indents at each depth with a separation of 1.5 μm between the rows and columns. The mean value of the elastic modulus as a function of distance from the coating/substrate interface was then calculated. Fig. 10(a) displays a sample elastic modulus profile from the array of indents at position 5 with the error bars representing the standard deviation of the four indents at each coating depth. It can be seen in Fig. 10(a) that the elastic modulus of the coating at this position increases from 130 GPa at the coating/substrate interface to 190 GPa at the coating surface.

Fig. 11(a) is a comparison between the coating elastic modulus measured using the photoacoustic microscopy system and nanoindentation at each measurement position. The elastic modulus displayed for nanoindentation represents the mean value of the indents made throughout the thickness of the coating at each position. From Fig. 11(a) it can be seen that the elastic modulus of the coating varies as a function of position; however, there is no general trend in the elastic modulus variation. The mean elastic modulus of the nine positions is 178.3 GPa for the photoacoustic measurements and 162.3 GPa for nanoindentation, resulting in an agreement between the two techniques that is within 9%. Fig. 11(b) is a comparison of the coating thickness measured using the photoacoustic microscopy system and observations with the optical microscope. Fig. 11(b) demonstrates that both techniques show a general trend of

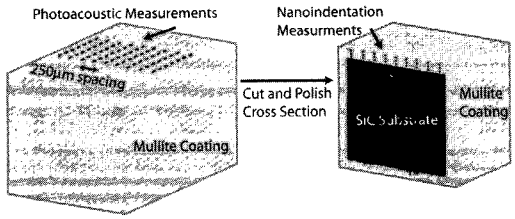

Fig. 9. Locations of the measurements on the selected side of the specimen.

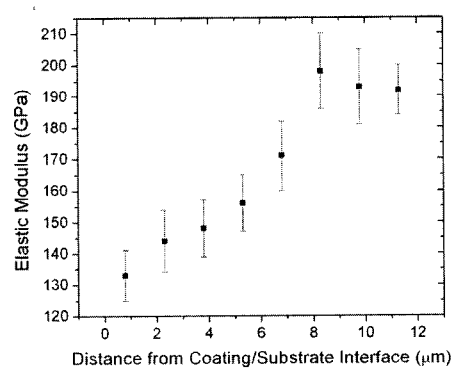

(a)

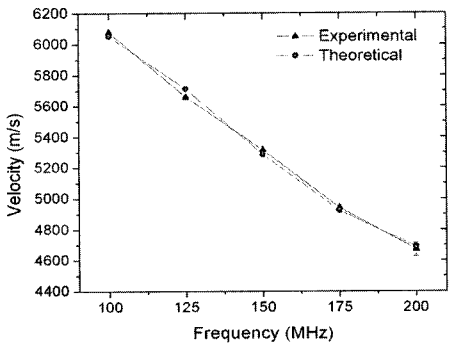

(b)

Fig. 10 (a) Depth distribution of the elastic modulus in the mullite coating from nanoindentation measurements at position 5. (b) Experimental and theoretical dispersion curve from position 9.

decreasing coating thickness from position 1 to position 9. The mean coating thickness of the nine positions is 13.4 μm for the photoacoustic measurements and 12.1 μm for the optical microscope observations, resulting in an agreement between the two techniques that is within 10%.

The thickness and effective elastic modulus results presented for each measurement technique show good general agreement. This indicates that the photoacoustic technique can be used to measure the effective elastic modulus and thickness variations across the surface of coatings that exhibit spatial variations in elastic properties. This offers the possibility of utilizing the photoacoustic microscopy system for feedback and optimization of the growth process, and perhaps ultimately incorporating such a system for *in-situ* process monitoring.

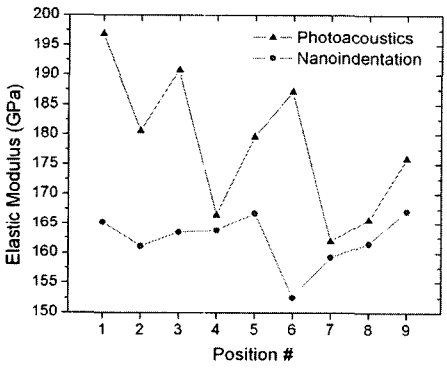

(a)

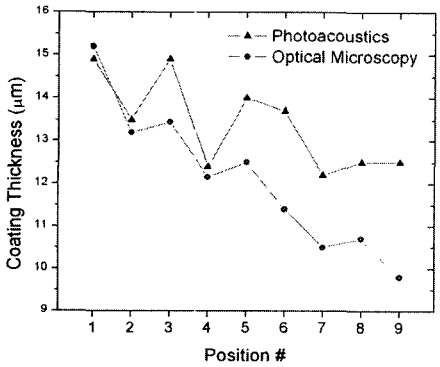

(b)

Fig. 11 (a) Comparison of the elastic modulus in the coating found using nanoindentation and photoacoustics. (b) Comparison of the coating thickness found using photoacoustics and the optical microscope.

4. Conclusions

A frequency domain photoacoustic microscopy system has been developed for the inspection of CVD mullite environmental barrier coatings grown on SiC substrates. The photoacoustic system used an amplitude modulated laser source for the generation of extremely narrowband SAWs. A photorefractive crystal based optical interferometry system was used for the detection of SAWs at frequencies up to 200 MHz. The coatings tested exhibited spatial variations in thickness and mechanical properties. Surface wave dispersion curves were used to extract an effective value for the elastic modulus and the thickness of the coating. Nanoindentation and optical microscopy were performed on polished coating cross-sections to validate the effective elastic modulus and thickness measurements, respectively. A comparison between the mean elastic modulus through the coating thickness found using nanoindentation, and the effective elastic modulus found using photoacoustics, resulted in agreement to within 9% between the techniques at different measurement locations on the coatings. A comparison of the coating thickness measured using optical microscopy and photoacoustics also showed general agreement between the techniques. The maximum discrepancy in the thickness found using these two approaches was approximately 14%. The photoacoustic measurements demonstrate the ability to monitor spatial variations in the elastic modulus and thickness of *as-grown* coatings, which can potentially provide valuable feedback for the optimization of the CVD growth process.

Acknowledgement

This work was supported by the National Science Foundation through grant DMR-0233952.

References

Alleyne, D., and Cawley, P. (1991) Two Dimensional Fourier Transform Method for the Measurement of Propagation Multi-Mode Signals, J. Acoust. Soc. Am., 89, pp. 1159-1168

Balogun, O., and Murray, T.W., (2006) A Frequency Domain Laser Based Ultrasonic System for Time Resolved Measurement of Broadband Acoustic Transients, J. Appl. Phys., 100, 034902

Bellan, C, and Dhers J. (2004) Evaluation of Young Modulus of CVD Coatings by Different Techniques, Thin Solid Films, 469–470, pp. 214–220

Berezina, S., Zinn, P., Schneider, D., Fei, D., and Rebinsky, D. (2004) Combining Brillion Spectroscopy and Laser-SAW Technique for Elastic Pproperty Characterization of Thick DLC Films, Ultrasonics, 43, pp. 87–93

Blouin, A., and Monchalin, J.-P. (1994) Detection of Ultrasonic Motion of a Scattering Surface by Two-Wave Mixing in a Photorefractive GaAs Crystal, Appl. Phys. Lett., 65, pp. 932–934

Briggs, A.D. (1992) *Acoustic Microscopy*, Clarendon Press, Oxford, pp. 15–294

Briggs, G.A.D. (1995) *Advances in Acoustic Microscopy*, Vol 1, Plenum Press, New York, pp. 153–217

Cheng, A., Murray, T.W., and Achenbach, J.D., (2001) Simulation of Laser-Generated Ultrasonic Waves in Layered Plates, J. Acoust. Soc. Am., 110, pp. 848-855

Delaye, P., Blouin, A., Drolet, D., Montmorillon, L.-A., Roosen, G., and Monchalin, J.-P. (1997) Detection of Ultrasonic Motion of a Scattering Surface by Photorefractive InP:Fe under an Applied dc Field, J. Opt. Soc. Am. B., 14, pp. 1723–1734

Doerner, M. F., and Nix, W. D. (1986) A Method for Interpreting the Data from Depth-Sensing Indentation Instruments, J. Mater. Res., 1, pp. 601–616

Duggal, A.R., Rogers, J.A., and Nelson, K.A. (1992) Real-Time Optical Characterization of Surface Acoustic Modes of Polyamide Thin-Film Coatings, J. Appl. Phys., 72, pp. 2823-2839

Farnell, G.W., and Adler, E.L. (1972) Elastic Wave Propagation in Thin Layers, Edited by W. P. Mason and R. N. Thurston, Academic, New York, Phys. Acoust., Vol. IX, pp. 35–127

Flannery, B.P., Press, W.H., Teukolsky, S.A., and Vettering, W. (1989) Numerical Recipes in C, Cambridge University Press, pp. 305-309

Guo Z. and Achenbach, J.D. (2000) Integration of Modelling and Acoustic Microscopy Measurements for Thin Films, J. Acoust. Soc. Am., 107(5), pp. 2462–2471

Hou, P., Basu, S.N., and Sarin, V.K. (2001) Structure and High-Temperature Stability of Compositionally Graded CVD Mullite Coatings, Int. J. Refract. Met. Hard. Mater., 19, pp. 467-477

Hurley, D.C., Tewary, V.K., and Richards, A.J. (2001) Surface Acoustic Wave Methods to Determine the Anisotropic Elastic Properties of Thin Films, Meas. Sci. Technol., 12, pp. 1486-1494

Ing, R. K., and Monchalin, J. -P. (1991) Broadband Optical Detection of Ultrasound by Two-Wave Mixing in a Photorefractive Crystal, Appl. Phys. Lett., 59, pp. 3233–3235

Ledbetter, H., Kim, S., Balzar, D., Crudele, S.,

and Kriven, W. (1998) Elastic Properties of Mullite, J. Am. Ceram. Soc., 81, pp. 1025-1028

Maris, H.J. (1997) Picosecond Ultrasonics, Scientific American, 278, pp. 64-67

Murray, T.W., and Balogun, O. (2004) High-Sensitivity Laser-Based Acoustic Microscopy Using a Modulated Excitation Source, Appl. Phys. Lett., 85(14), pp. 2974-2976

Murray, T.W., Balogun, O., Steen, T.L., Basu, S.N., and Sarin, V.K. (2005) Inspection of Compositionally Gmullite Coatings Using Laser Based Ultrasonics, Int. J. Refract. Met. Hard. Mater., 23, pp. 322-329

Neubrand, A., Hess, P. (1992) Laser Generation and Detection of Surface Acoustic Waves: Elastic Properties of Surface Layers, J. Appl. Phys., 71, pp. 227-238

Ohmura, T., and Matsuoka, S. (2003) Evaluation of Mechanical Properties of Ceramic Coatings on a Metal Substrate, Surf. Coat. Technol., 169-170, pp. 728–731

Oliver, W.C. and Pharr, G.M. (1992) An Improved Technique for Determining Hardness and Elastic Modulus Using Load and Displacement Sensing Indentation Experiments, J. Mater. Res., 7, pp. 1564-1583

Richardson, C.J.K., Ehrlich, M.J., and Wagner, J.W. (1999) Interferometric Detection of Ultrafast Thermoelastic Transients in Thin Films: Theory with Supporting Experiment, J. Opt. Soc. Am. B, 16(6), pp. 1007-1015

Rogers, J.A., Fuchs, M., Banet, M.J., Hanselman, J.B., Logan, R., and Nelson, K.A. (2000) Optical Generation and Characterization of Acoustic Waves in Thin Films, Annu. Rev. Mater. Sci., 30, pp. 117–157

Vaz, F., Carvalho, S., Rebouta, L., Silva, M.Z., Paul, A. and Schneider, D. (2002) Young's Modulus of (Ti,Si)N Films by Surface Acoustic Waves and Indentation Techniques, Thin Solid Films, 408, pp. 160-168

Zhang, F., Krishnaswamy, S., Fei, D., Rebinsky, D.A., and Feng, B. (2006) Ultrasonic Characterization of Mechanical Properties of Cr- and W-Doped Diamond-Like Carbon Hard Coatings, Thin Solid Films, 503, pp. 250-258

Ziebert, C., Ye, J.,Sell, K. and Ulrich, S. (2006) High-Resolution Depth Profiling of Mechanical Properties of Thick Cubic Boron Nitride Coatings, Surf. Coat. Technol., 200, pp. 6454-6458